

Why ice is so slippery

Sigbjørn Løland Bore,^{1,*} B.N.J. Persson,^{2,3,4,†} and Henrik Andersen Sveinsson^{5,‡}

¹*Hylleraas Centre for Quantum Molecular Sciences, Department of Chemistry,
University of Oslo, PO Box 1033 Blindern, 0315 Oslo, Norway*

²*State Key Laboratory of Solid Lubrication, Lanzhou Institute of Chemical Physics,
Chinese Academy of Sciences, 730000 Lanzhou, China*

³*Peter Grünberg Institute (PGI-1), Forschungszentrum Jülich, 52425, Jülich, Germany*

⁴*MultiscaleConsulting, Wolfshovener str. 2, 52428 Jülich, Germany*

⁵*The Njord Centre, Department of Physics, University of Oslo, PO Box 1048 Blindern, 0316 Oslo, Norway*

(Dated: March 13, 2026)

The origin of ice’s slipperiness has long puzzled scientists. To resolve this question, we simulate ice–glass (amorphous silica) friction at the nanoscale from first principles and upscale to the macroscale using a frictional heating model. We find that nanoscale simulations alone cannot capture the correct velocity dependence of ice friction, resulting in an overestimated coefficient of friction. By properly accounting for frictional heating, we find a strong increase in contact temperature toward the melting point, even under modest motion of 1 millimeter with velocities above 0.1 m/s, yielding excellent agreement with experimental friction data across a wide range of velocities. While the initial formation of a lubricating film on ice may occur without heating, the ultimate slipperiness of ice hinges on frictional heating, as proposed by Bowden and Hughes in 1939, but without incorporating melting.

The interest in ice friction has ancient roots, with early human activity involving sliding on ice from around 10000 B.C. using sleds [1]. On this historical timescale, it was only very recently that the first scientific explanation for ice slipperiness was put forward in the 1800s by Michael Faraday’s observations of premelting [2, 3]: a liquid pre-melting film spontaneously forms on ice and provides lubrication. This explanation was followed by John Joly’s pressure-melting theory [4]: pressure causes a melting point depression, creating a lubricating premelting film. Subsequently, Bowden and Hughes proposed that the low friction of ice results from frictional heating [5]: friction between a moving object on ice, such as a skate blade, generates heat, creating a thin film of liquid water on the ice surface. This meltwater film acts as a lubricant, significantly reducing friction and enabling the smooth gliding motion characteristic of ice skating.

Modern science continues to debate. On the experimental side, Canale *et al.* emphasized the nanorheology of ice friction, finding a lubricating layer consisting of a viscous slurry of ice nanoparticles in water [6]. Weber *et al.* combined friction experiments with MD simulations, attributing ice slipperiness to highly mobile water molecules at the ice surface [7]. Liefferink *et al.* followed up, investigating the roles of temperature, pressure, and velocity, proposing a ploughing mechanism [8]. They concluded that the friction coefficient is not very sensitive to frictional heating. On the theoretical side, advances in computational efficiency have enabled molecular dynamics (MD) studies of nanoscale ice friction. Using force-field MD simulations, Baran *et al.* found the premelting film to be a robust phenomenon, reporting shear thinning and large slip lengths at hydrophobic interfaces as crucial for low ice friction, arguing for a minor role of frictional heating due to low film viscosity [9, 10]. More recently, Atila *et*

al. performed ice sliding on ice MD simulations, proposing a mechanism for displacement-driven amorphization at low temperatures [11]. Their MD shows that a relatively thick (10 nm) liquid-like film can form at ice interfaces during slip with negligible temperature rise, through a competition between shear-induced amorphization and recrystallization. When sliding stops, the film recrystallizes, leaving only a few interfacial monolayers in non-ice configurations set by the counter-surface. From these conflicting views, it can be concluded that no consensus has been reached on *why ice is so slippery*.

In this paper, we present evidence that indicates frictional heating is the primary cause of ice slipperiness. Applying machine learning interatomic potentials based MD, we simulate nanoscale ice friction against a realistic ice–glass (amorphous silica) interface—a model system for ice–rock contacts in nature—from first principles (see Figure 1a and the Supplemental Material [12] for details). By integrating our nanoscale MD findings into the frictional heating model developed by Persson [13], we predict the macroscopic ice friction behavior. Comparing our macroscale predictions with experimental ice–glass friction data, we find excellent agreement, strongly supporting the frictional heating theory of Bowden and Hughes.

The key control parameters in ice friction experiments are the background temperature T_0 of the ice and the velocity v of the sliding body. Direct prediction of experimental ice friction conditions using MD is impossible due to the large length and time scales involved. However, from nanoscale MD simulations, we can obtain the frictional shear stress $\sigma_f(v, T)$ acting in the asperity contact regions for given sliding velocity v and contact temperature T [12]. We perform such simulations of the ice–glass contact (Figure 1a), for $v \gtrsim 0.01$ m/s, with the

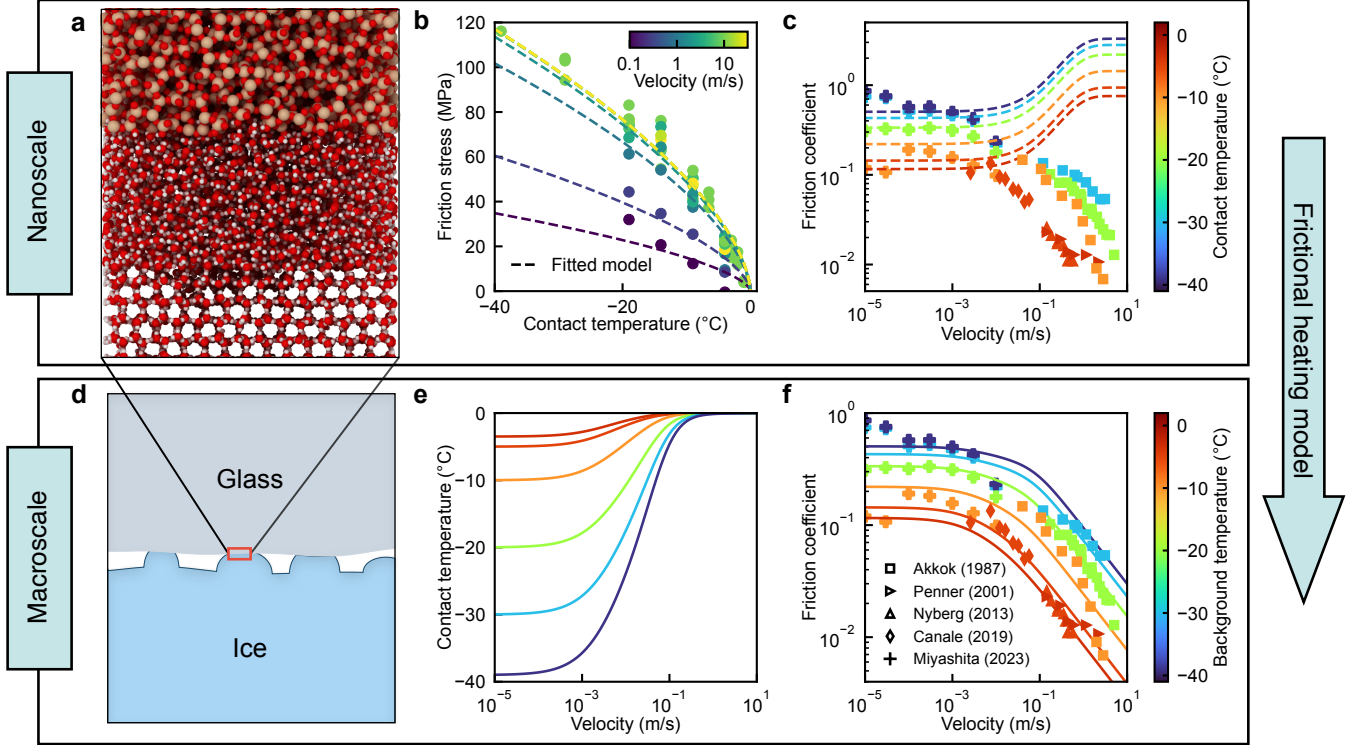


Figure 1 | Nanoscale vs. macroscale ice friction. **a** Setup for nanoscale MD simulations of amorphous silica sliding on ice. **b** Friction stress as a function of contact temperature for different sliding velocities from nanoscale MD simulations, with fitted equation (1) (dashed lines). **c** Ice friction coefficient as a function of velocity for different temperatures with equation (1) directly, without frictional heating, comparing with experiments. **d** Illustration of macroscale friction, where nanoscale represents one asperity contact. **e** Contact temperature as a function of velocity for different background temperatures using the frictional heating model (equation (4)). **f** Macroscale ice friction coefficient using the frictional heating model, comparing with experiments. Contact temperatures for nanoscale MD simulations are reported in °C relative to the DC-R²SCAN model melting point of 289 K. Experimental friction coefficient data are from ice–glass friction experiments [6, 14, 15] and curling stone experiments [16, 17], which is composed of granite with ~70% content of silica.

friction stress shown in Figure 1b. The friction stress from nanoscale MD is well-modeled by the following expression:

$$\sigma_f(v, T) = \sigma_k \left(1 - \frac{T}{T_m}\right)^\beta \left[1 - \left(1 - \frac{\sigma_c}{\sigma_k}\right) e^{-\frac{v}{v_k}}\right], \quad (1)$$

where $\sigma_c = 60$ MPa has been chosen based on experimental ice–glass friction data [14] and $\sigma_k = 391$ MPa, $v_k = 0.54$ m/s and $\beta = 0.61$ on our nanoscale MD simulation data for $v \geq 0.01$ m/s, with parameterization details provided in the Methods below. Equation (1) can be rationalized as a sigmoid between two limiting behaviors:

$$\sigma_f(v, T) = \sigma_c \left(1 - \frac{T}{T_m}\right)^\beta, \quad v \ll v_k, \quad (2)$$

$$\sigma_f(v, T) = \sigma_k \left(1 - \frac{T}{T_m}\right)^\beta, \quad v \gg v_k, \quad (3)$$

representing lower and upper velocity limits, respectively. Equation (2) has previously been proposed by Persson for

ice–ice friction experiments for low velocities [13], albeit with $\beta = 0.15$.

To incorporate heat transport effects, we use a frictional heating model. By assuming that ice and glass make contact at asperities, making up only a small fraction of the apparent contact area (Figure 1d), the contact temperature can be expressed as [13, 18] (see Methods below for additional details):

$$T = T_0 + \sigma_f(v, T) \frac{s(v)vR}{\kappa} \left(1 + \frac{\pi Rv}{8D}\right)^{-\frac{1}{2}}. \quad (4)$$

Here, R is the asperity contact radius, D is the thermal diffusivity, κ is the thermal conductivity, all of which are available from literature data (see Table 1). $s(v)$ is the proportion of heat that is absorbed by the slider, and can be explicitly expressed as a function of the sliding velocity (see Methods below), typically in the range from 0.6 to 1 with increasing sliding velocity. By inserting equation (1) into equation (4), we obtain an implicit equation for the

contact temperature at a given background temperature and sliding velocity, which we solve iteratively to obtain T and σ_f . The friction coefficient can then be estimated from friction stress as $\mu = \sigma_f / \sigma_P$, by assuming contact pressure equals ice penetration hardness, with $\sigma_P \approx 35$ MPa (see Methods below).

Figure 1c reports the nanoscale ice friction coefficient as a function of sliding velocity for different temperatures, using the nanoscale MD results directly. Clearly, when compared with experimental ice friction data, the coefficient of friction is not only grossly overestimated in magnitude but also shows the wrong trend: friction increasing with sliding velocity, in opposition to experiments. Using the frictional heating model described by equation (4), we can upscale nanoscale MD results to the macroscale. The resulting contact temperature is reported in Figure 1e. At low velocities, frictional heating is negligible, with the contact temperature close to the background temperature. At higher velocities, frictional heating increases the contact temperature, which approaches the melting point for a sliding velocity of around 0.1 m/s. This change in contact temperature dramatically changes the ice friction coefficient behavior from the nanoscale ice friction coefficients in Figure 1c to the macroscale ice friction coefficients in Figure 1f, which shows excellent agreement with experimental data [6, 14–17], having an R^2 coefficient of determination of 0.83 (see Figure 3).

From the nanoscale MD simulations, we can extract properties of the premelting film, which we can also upscale to the macroscale using the frictional heating model. In Figure 2a, we report the premelting film thickness as a function of sliding velocity. While the premelting film thickness increases with sliding velocity at the nanoscale, the effect is significantly amplified at the macroscale, rising by about an order of magnitude. This amplification is also evident when considering viscosity, which drops by about two orders of magnitude. It is these two effects combined that cause the strong drop in ice friction with increasing sliding velocity at the macroscale.

Our findings provide a window into reconciling conflicting views on ice friction present in the literature. Baran *et al.* [9, 10] highlight shear thinning as important for ice friction. We also observe it in our nanoscale simulations (Figure 2b). Atila *et al.* [11] put forward displacement-driven amorphization as a mechanism for the formation of the liquid film. This mechanism is likely at play in our nanoscale simulations. In fact, our frictional heating model does not incorporate true thermal melting: there is no melting enthalpy, and the friction stress in equation (1) decreases continuously as $(1 - T/T_m)^\beta$ without a phase transition. Premelting is also important, as it gives rise to the disordered interface in the first place. However, even with these effects present, we have shown that nanoscale simulations do not capture the velocity dependence of ice friction (Figure 1c), and that frictional heating is a necessary ingredient to describe the phenomenon qual-

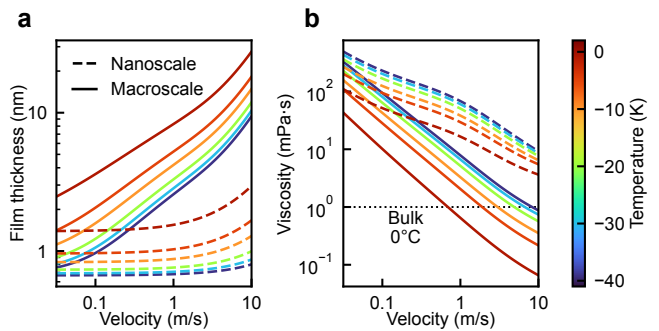


Figure 2 | Nanoscale vs. macroscale premelting film properties. **a** premelting film thickness and **b** viscosity estimated directly from nanoscale MD simulations, and to macroscale using the frictional heating model. Nanoscale is reported for contact temperature, while macroscale is reported for background temperature.

itatively and quantitatively. Finally, pressure melting is already considered unlikely in most situations, as ice asperity contact regions yield by plastic flow before the pressure becomes high enough to form liquid water, and our results corroborate that this is indeed an unnecessary hypothesis to explain the slipperiness of ice.

Several aspects of ice friction remain to be explored. We have not considered in depth the effects of surface chemistry, such as hydroxylated or hydrophobic surfaces (e.g., waxes used in skiing), snow, ploughing [8], or the formation of ice-particle slurries. Canale *et al.* [6] report a liquid film of order ~ 100 nm with viscosity much larger than that of bulk water, suggestive of a hydrodynamic slurry regime distinct from the thin-film boundary lubrication modeled here. Nevertheless, the velocity dependence of the friction coefficient data by Canale *et al.* is consistent with our predictions (Figure 1f). Similarly, materials with higher thermal conductivity, such as metals, would lead to different thermal feedback. These are promising directions for future work, requiring additional simulations and different theoretical frameworks.

Our analysis focuses on the velocity dependence of ice friction, but as emphasized by Rosenberg, ice is slippery even while standing still [19], potentially at odds with frictional heating hypotheses. This paradox is resolved by the picture we provide here. Very small movements persisted at the scale of one millimeter with tangential velocities of ~ 0.1 m/s lead to dramatic drops in friction. This is in close agreement with everyday experience: Slow, careful steps below this velocity threshold retain grip, while rapid scuffing to regain grip ends in catastrophe.

* s.l.bore@kjemi.uio.no

† b.persson@fz-juelich.de

‡ h.a.sveinsson@fys.uio.no

- [1] R. M. Gramly, *Guide to Palaeolithic Artifacts and Features of the Americas* (Bloomsbury Publishing USA, 2024) p. 95.
- [2] Faraday, The London, Edinburgh, and Dublin Philosophical Magazine and Journal of Science **17**, 162 (1859).
- [3] H. H. G. Jellinek, Journal of colloid and interface science **25**, 192 (1967).
- [4] J. Joly, Scientific Proceeding of the Royal Dublin Society, New Series **5**, 453 (1887).
- [5] F. P. Bowden and T. Hughes, Proceedings of the Royal Society of London. Series A. Mathematical and Physical Sciences **172**, 280 (1939).
- [6] L. Canale, J. Comtet, A. Niguès, C. Cohen, C. Clanet, A. Siria, and L. Bocquet, Physical Review X **9**, 041025 (2019).
- [7] B. Weber, Y. Nagata, S. Ketzetzi, F. Tang, W. J. Smit, H. J. Bakker, E. H. G. Backus, M. Bonn, and D. Bonn, The Journal of Physical Chemistry Letters **9**, 2838 (2018).
- [8] R. W. Liefferink, F. C. Hsia, B. Weber, and D. Bonn, Physical Review X **11**, 011025 (2021).
- [9] L. Baran, P. Llombart, W. Rzyśko, and L. G. MacDowell, Proceedings of the National Academy of Sciences **119**, e2209545119 (2022).
- [10] L. Baran and L. G. MacDowell, The Journal of Chemical Physics **160**, 054702 (2024).
- [11] A. Atila, S. V. Sukhomlinov, and M. H. Müser, Physical Review Letters **135**, 066204 (2025).
- [12] See Supplemental Material for detailed a description of methods for nanoscale modeling.
- [13] B. N. J. Persson, The Journal of chemical physics **143**, 224701 (2015).
- [14] N. Miyashita, A. E. Yakini, W. Pyckhout-Hintzen, and B. N. J. Persson, The Journal of Chemical Physics **158**, 174702 (2023).
- [15] M. Akkok, C. M. McC. Ettles, and S. J. Calabrese, Journal of Tribology **109**, 552 (1987).
- [16] A. R. Penner, American Journal of Physics **69**, 332 (2001).
- [17] H. Nyberg, S. Alfredson, S. Hogmark, and S. Jacobson, Wear **301**, 583 (2013).
- [18] J. A. Greenwood, Wear **150**, 153 (1991).
- [19] R. Rosenberg, Physics Today **58**, 50 (2005).
- [20] B. N. J. Persson, A. I. Volokitin, and H. Ueba, Journal of Physics: Condensed Matter **23**, 045009 (2011).
- [21] J. Li, S. Li, W. Zhang, B. Wei, and Q. Yang, Lubricants **10**, 265 (2022).
- [22] M. M. Miranda, C. R. Matos, N. V. Rodrigues, A. J. S. C. Pereira, and J. J. Costa, Journal of Iberian Geology **45**, 147 (2019).
- [23] P. V. Hobbs, Oxford: Clarendon Press (1974).
- [24] D. T. Limmer and D. Chandler, The Journal of chemical physics **141** (2014).
- [25] S. Dasgupta, E. Lambros, J. P. Perdew, and F. Paesani, Nature Communications **12**, 6359 (2021).
- [26] S. Dasgupta, G. Cassone, and F. Paesani, The Journal of Physical Chemistry Letters **16**, 2996 (2025).
- [27] S. Dasgupta, S. Saha, and F. Paesani, The Journal of Physical Chemistry Letters **16**, 11996 (2025).
- [28] J. Zeng *et al.*, The Journal of Chemical Physics **159**, 054801 (2023).
- [29] J. Zeng, D. Zhang, A. Peng, X. Zhang, S. He, Y. Wang, X. Liu, H. Bi, Y. Li, C. Cai, *et al.*, Journal of Chemical Theory and Computation **21**, 4375 (2025).
- [30] Y. Zhai, A. Caruso, S. L. Bore, Z. Luo, and F. Paesani, The Journal of Chemical Physics **158**, 084111 (2023).
- [31] S. L. Bore and F. Paesani, Nature Communications **14**, 3349 (2023).
- [32] F. Sciortino, Y. Zhai, S. L. Bore, and F. Paesani, Nature Physics **21**, 480 (2025).
- [33] Hylleraas Active Learning, <https://gitlab.com/hylleraasplatform/hyal> (2025).
- [34] H. M. Cezar, T. Bodenstern, H. A. Sveinsson, M. Ledum, S. Reine, and S. L. Bore, npj Computational Materials **11**, 200 (2025).
- [35] M. Matsumoto, T. Yagasaki, and H. Tanaka, Journal of Computational Chemistry **39**, 61 (2018).
- [36] L. C. Erhard, J. Rohrer, K. Albe, and V. L. Deringer, npj Computational Materials **8**, 90 (2022).
- [37] D. Heyes, E. Smith, D. Dini, and T. Zaki, The Journal of chemical physics **135**, 024512 (2011).
- [38] A. Brünger, C. L. Brooks III, and M. Karplus, Chemical physics letters **105**, 495 (1984).
- [39] M. Holz, S. R. Heil, and A. Sacco, Physical Chemistry Chemical Physics **2**, 4740 (2000).
- [40] A. J. Easteal, W. E. Price, and L. A. Woolf, Journal of the Chemical Society, Faraday Transactions 1: Physical Chemistry in Condensed Phases **85**, 1091 (1989).
- [41] R. Mills, The Journal of Physical Chemistry **77**, 685 (1973).
- [42] E. W. Lemmon, M. O. McLinden, and D. G. Friend, in *NIST Chemistry WebBook*, edited by P. Linstrom and W. Mallard (National Institute of Standards and Technology, Gaithersburg, MD, 2021).
- [43] A. Dehaoui, B. Issenmann, and F. Caupin, Proceedings of the National Academy of Sciences **112**, 12020 (2015).
- [44] A. Musaelian, S. Batzner, A. Johansson, L. Sun, C. J. Owen, M. Kornbluth, and B. Kozinsky, Nature Communications **14**, 579 (2023).
- [45] P. M. Larsen, S. Schmidt, and J. Schiøtz, Modelling and Simulation in Materials Science and Engineering **24**, 055007 (2016).
- [46] A. Stukowski, Modelling and simulation in materials science and engineering **18**, 015012 (2009).

METHODS

Frictional heating modeling

We determine the contact temperature at the ice surface and the slider due to frictional heating as follows. We assume that the slider is flat and that it makes contact with the ice substrate only at isolated pebble-shaped asperities of radius R . These asperities make up only a small proportion of the apparent contact area, as illustrated in Figure 1d. Due to frictional heating, there will be an increase ΔT of the contact temperature T with respect to the background temperature T_0 . Seen from the slider, the contacts with the ice pebbles of the substrate are disk-shaped moving heat sources that provide a heat flux J . The maximum temperature increase within the contact region is, in this case, very well approximated by

equation (8) in Ref. [18]:

$$\Delta T = \frac{s(v)JR}{\kappa_{\text{slider}}} \left(1 + \frac{\pi}{8} \frac{Rv}{D_{\text{slider}}} \right)^{-1/2}, \quad (5)$$

D is the thermal diffusivity, κ is the thermal conductivity, and s is the proportion of the heat that goes into the slider (the rest, $1-s$, goes into the ice). This expression includes both the effect of normal heat transfer away from the contact and the effect of new cold glass constantly entering the contact region. It is useful to write equation (5) as

$$s(v)J = \alpha_{\text{slider}} \Delta T \quad (6)$$

with

$$\alpha_{\text{slider}} = \frac{\kappa_{\text{slider}}}{R} \left(1 + \frac{\pi}{8} \frac{Rv}{D_{\text{slider}}} \right)^{1/2}. \quad (7)$$

For the substrate, with stationary ice pebbles, the maximum temperature elevation is [18]:

$$\Delta T = \frac{(1-s(v))JR}{\kappa_{\text{substrate}}}, \quad (8)$$

or equivalently

$$(1-s(v))J = \alpha_{\text{substrate}} \Delta T, \quad (9)$$

with

$$\alpha_{\text{substrate}} = \frac{\kappa_{\text{substrate}}}{R}. \quad (10)$$

We approximate the temperatures on the ice surface and the silica glass surface to be equal (i.e., the contact temperature) [20]. We thus obtain the partitioning coefficient of the heat flux:

$$s(v) = \frac{\alpha_{\text{slider}}}{\alpha_{\text{substrate}} + \alpha_{\text{slider}}}. \quad (11)$$

This partitioning tends towards 0.5 for stationary contacts between materials with similar thermal properties, whereas it tends towards 1 at high sliding velocities, meaning almost all the heat goes into the slider. Using the MD-derived friction law in equation (1), we insert $J = \sigma_f v$ into equation (5) to recover the contact temperature relation given in equation (4). Since σ_f is a function of the contact temperature, equation (4) is an implicit equation for the contact temperature T in the region. We solve it iteratively and then obtain σ_f from the same constitutive relations. Note that we do not consider squeeze-out of the liquid film, as for nanometer-thick films at macroscopic contact dimensions, squeeze-out is negligible even at the low viscosity of water. In addition, during sliding, shear-induced amorphization would continuously produce a liquid-like film on the ice surface [11].

To obtain friction stresses for comparison with experiments, we insert parameters taken from the curling literature, because typical curling ice has been very well characterized; it is pebbled with a contact diameter of around

2 mm [21]. To obtain roughly the midpoint temperature instead of the maximum temperature of the contacts, we set $R = 0.5$ mm. Curling stones have a very flat contact surface, which is consistent with the heat model described above. These stones are made of granite, which is mostly a silicate mineral, for which our amorphous silica glass is a reasonable analogue. In the frictional heating model, we use thermal properties of the ice and granite as listed in Table 1. We compute the thermal diffusivity needed in equation (4) by $D = \kappa/(\rho C_P)$.

Table 1 | Material properties used in the frictional heating model. Granite properties were obtained from Ref. [22], and ice properties from Ref. [23].

Property	Unit	Ice	Granite
Thermal conductivity κ	(W m ⁻¹ K ⁻¹)	2.2	3.2
Density ρ	(g cm ⁻³)	0.917	2.7
Specific heat C_P	(J kg ⁻¹ K ⁻¹)	2100	800

Friction coefficient

Relating the frictional shear stress to the friction coefficient is nontrivial because it depends on whether the surfaces deform elastically (as expected for sufficiently smooth surfaces) or plastically. Plastic deformation of ice is a stress-aided, thermally activated process, and the penetration hardness of ice depends on the temperature and the indentation velocity. Here we note that if a slider is slid repeatedly on ice, the high ice asperities will be smoothed plastically during the first few sliding events, so after run-in, the surfaces may deform only elastically, and subject to a normal stress on the order of the penetration hardness of ice of about $p_H = 35$ MPa, collected from experimental data [16, 23]. We then compute the friction coefficient $\mu = \sigma_f/\sigma_P$

Ice–glass friction model parameterization

We represent our nanoscale MD data by analytical functions parameterized based on nanoscale ice–glass friction data at specific state points. Because the melting point of our DC-R²SCAN water model is 289 K (see Methods), we report temperatures relative to this melting point in °C to enable comparison with experimental data. For equation (1), we fitted the parameters σ_k , v_k , β , and γ to nanoscale MD data for friction stress as a function of temperature and sliding velocity at a contact pressure of 10 MPa, having set σ_c based on experimental ice–glass friction coefficient data from Ref. [14], as the accuracy of our nanoscale MD simulations at low velocities is limited (see Supplemental Material [12] for details). Parity plots of how well the model predictions match the MD data

are shown in Figure 3a, and how macroscale predictions match the experimental friction coefficient in Figure 3b. For the premelting film thickness, we fitted the following functional form for simulations with temperatures between 260 and 289 K:

$$h(v, T) = h_0 + a \left[-\ln \left(1 - \frac{T}{T_m} \right) \right]^\gamma \left(1 + \frac{v}{v_0} \right), \quad (12)$$

where $h_0 = 0.72$ nm, $a = 5.00$ pm, $\gamma = 2.66$, $v_0 = 2.89$ m s⁻¹ are fitted to MD data for premelting film thickness as a function of temperature and sliding velocity, with parity plot in Figure 3c. We note that Limmer and Chandler proposed such a logarithmic dependence for temperature for premelting thickness in ice–air [24], albeit without γ exponent. A parity plot of how well the model predictions match the MD data is reported in Figure 3c. Equation (12) is plotted in Figure 2a, with premelting film viscosity in Figure 2b computed using $\eta = \sigma_f h/v$.

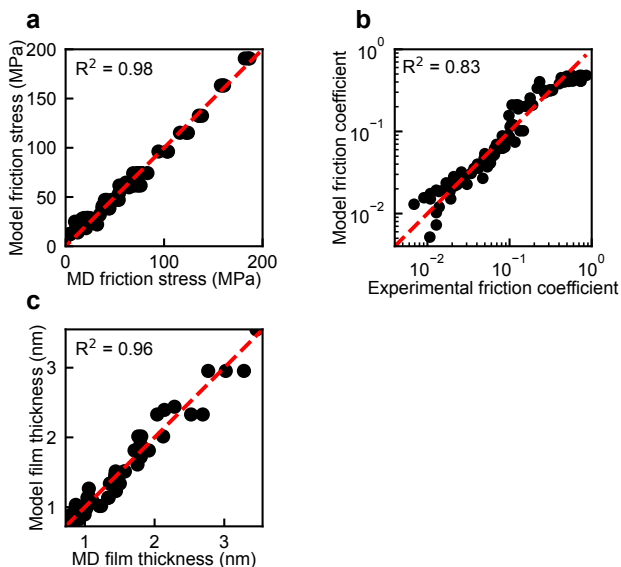


Figure 3 | Parity plots for ice–glass friction modeling vs. data. **a** Nanoscale MD data vs. fitted model predictions for friction stress equation (1), corresponding to Figure 1b. **b** Experimental vs. modeled macroscale friction coefficient, corresponding to Figure 1f. **c** MD data vs. fitted model predictions for premelting film thickness, corresponding to Figure 2a.

ACKNOWLEDGMENTS

This work was supported by the Research Council of Norway through the Centre of Excellence Hylleraas Centre for Quantum Molecular Sciences (Grant 262695) and the Young Researcher Talent grants 344993 and 354100. We acknowledge the EuroHPC Joint Undertaking for awarding this project access to the EuroHPC

supercomputer LUMI, hosted by CSC (Finland) and the LUMI consortium through a EuroHPC Regular Access call (Grants EHPC-REG-2023R02-088, EHPC-REG-2023R03-146). Support was also received from the Centre for Advanced Study in Oslo, Norway, which funded and hosted the SLB Young CAS Fellow research project during the academic years of 23/24 and 24/25. Part of the simulations were performed on resources provided by Sigma2 — the Norwegian National Infrastructure for High-Performance Computing and Data Storage (grant numbers NN4654K and NS4654K). Generative AI (Claude Opus 4, Anthropic) was used to assist with manuscript editing and revision. All authors have reviewed and take full responsibility for the content.

SUPPLEMENTAL MATERIAL

METHODS FOR NANOSCALE MODELING

This document details the molecular dynamics methodology used to generate the nanoscale ice friction data discussed in the main text.

First principles approach

To model nanoscale ice–glass friction from first principles accurately, we describe the electronic structure using density-corrected density-functional theory (DC-DFT) with the R²SCAN functional (DC-R²SCAN). DC-DFT has been extensively benchmarked for water, showing not only excellent correspondence in energies with respect to coupled cluster calculations, but also for liquid water properties [25–27]. The atomic core electrons were described using Goedecker–Teter–Hutter (GTH) pseudopotentials, while valence electron molecular orbitals were expanded in triple-zeta double-polarized basis sets (TZV2P) optimized for the SCAN functional. The kinetic energy cutoff for the plane-wave expansion of the density was set to 2500 Ry, which was required to get a numerical accuracy of ~ 2 meV/Å for forces. The truncated Coulomb operator with a cutoff radius 6 Å was used, corresponding to approximately half the length of the smallest edge of the simulation cell. To overcome the computational cost of the Hartree–Fock calculation, the alternating direction method of multipliers (ADMM) approximation was used with an optimized valence basis set (BASIS_ADMM_UZH). The Schwarz integral screening threshold was set to 10^{-6} atomic units, starting from a converged PBE calculation.

Machine learning interatomic potential

To enable nanoscale ice–glass friction simulations from first principles with DC-R²SCAN at system sizes of thousands of atoms and timescales up to hundreds of nanoseconds, we trained computationally efficient machine-learning interatomic potentials (MLIPs) to reproduce DC-R²SCAN energies and forces. As the MLIP, we used DeePMD [28, 29] with the se_e2_a architecture and 25, 50, or 100 neurons for the hidden embedding layer, and a 16-neuron submatrix of the embedding matrix. A distance cutoff of 6 Å was used with a smoothing region of 0.5 Å. The potential is represented by a fully connected deep neural network with three layers of 240 neurons each. These are standard settings, which have also been used to study the phase diagram of water [30–32]. To train the MLIP, we built a training set by adversarial active learning implemented in the HyAL code [33] and documented in [34]. In brief, our adversarial active-learning

approach is iterative: successive MLIPs are used to extend the training set by adding adversarial (high-error) structures, yielding robust and accurate MLIPs [34]. To ensure that the MLIP accurately describes interfaces and confined water under shear, not only bulk properties, the training set includes structures extracted from sheared ice–silica MD simulations. The complete training set comprises 1164 structures, including ice Ih, liquid water, liquid–ice coexistence, amorphous silica, silica–water, and sheared ice–silica interfaces, and is openly available in the associated data repository.

Protocol for nanoscale ice–glass friction simulations

The initial simulation box shown in Figure S1 is prepared in three steps. First, a block of hexagonal ice is generated using GENICE to ensure the correct proton disorder [35], with its cell geometry scaled to the equilibrium geometry at 0.1 MPa and temperature T , with basal plane orientation at the surface. Second, we create an amorphous silica slab by melting beta-cristobalite at 5000 K, deforming the box to perfectly match the ice equilibrium geometry’s L_x and L_y , and then quenching down from 4000 K to T with a quench rate of 1×10^{12} K/s, a rate that has been shown previously to yield converged amorphous silica structures [36]. Third, these two parts are combined with an offset of 1 Å to create an interface with a small gap in between. Finally, we perform equilibration under constant contact pressure P_N . To perform constant contact pressure simulations, we freeze 3 Å of the bottom ice layer and rigidify the top 3 Å of the top amorphous layer, constraining forces to the z -direction only, applying a force on each atom [37]:

$$F_z = -\frac{P_N L_x L_y}{N_{\text{atoms,rigid}}} \quad (\text{S1})$$

All data presented here were obtained from simulations carried out with 10 MPa contact pressure. We maintain temperature by thermostating 36 Å and 17 Å of the ice and silica, respectively, using a Langevin thermostat with a time constant of 100 fs [38], correcting for the net center-of-mass motion contribution to the temperature. The thermostat is applied only to atoms far from the sliding interface, ensuring that it does not damp the sliding motion or bias the friction stress. After equilibration of 5 ns, we apply a constant velocity to the rigid object in the x direction. By setting the forces to zero in the x and y directions, we maintain the sliding velocity in the x direction.

Validation of DC-R²SCAN MLIP

To assess the accuracy of our DC-R²SCAN MLIP, we validated it for physical properties of water and silica in

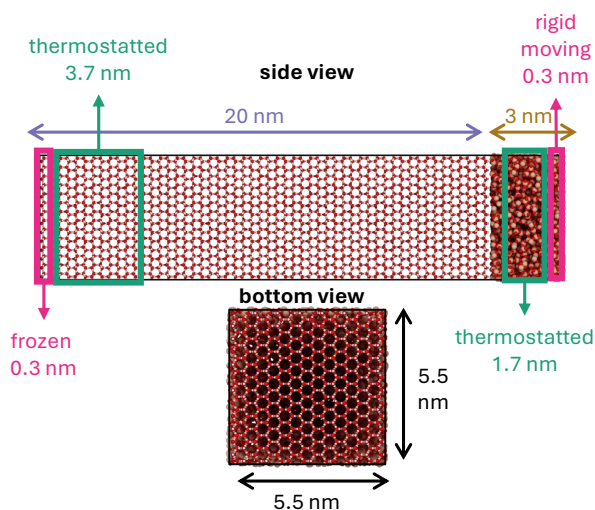


Figure S1 | Setup for nanoscale ice-glass simulations.

Figure S2. The radial distribution function predicted by DC-R²SCAN (Figure S2a) closely follows experiment, indicating an accurate liquid structure. The density isobars in Figure S2b show that the ice density is well reproduced, whereas the liquid-water density is underestimated by about 5%. In a separate publication [34], we computed the water density for DC-R²SCAN at 0.1 MPa and 300 K using an Allegro-based MLIP (Table S1); the present value agrees within 0.2%, indicating well-converged training data. Direct coexistence (Figure S2c) yields a melting point of 289 K, i.e. 17 K above experiment. The amorphous-silica structure factor (Figure S2f) agrees well with experiment and a DFT-based GAP model for both quench rates [36], with a slight underestimation of the first peak.

Table S1 | Benchmark of DC-R²SCAN MLIP. All properties are reported for 300 K, 0.1 MPa, except for melting point. Ref. 34 uses DC-R²SCAN, but with the Allegro MLIP architecture and different training set structures [44].

Property	Unit	This work	Ref. 34	Experiment
Density	(g/cm ³)	0.948(1)	0.950(9)	0.996
Melting point	(K)	289(2)	—	273.15
Diffusion	(10 ⁻⁹ m ² /s)	1.8(2)	1.59(9)	2.4021
Viscosity	(mPa · s)	0.7868	—	0.8536

MD data analysis protocols

The raw time series for friction stress and premelting film thickness are shown in Figure S4 and Figure S3.

Averages for steady state are computed from the time series after an initial transient period of 5 ns. As shown in Figure S4 and Figure S3, the liquid film grows from the initial interface upon the onset of sliding, reaching a steady state within nanoseconds. This initial time evolution is similar to that reported for displacement-driven amorphization by Atila et al. [11]. The steady-state film thickness and friction stress depend on contact temperature and sliding velocity, and serve as inputs to the macroscale frictional heating model.

The premelting film thickness was estimated using the Polyhedral template matching [45] of OVITO [46]. Specifically, for each oxygen, we computed the Polyhedral template-matching RMSD for cubic and hexagonal diamond, and assigned it as ice-like if $0.01 < \text{RMSD} < 0.25$. Then, using a histogram and fitting the function $f(z)$:

$$f(z) = \frac{A}{2} \left[1 - \tanh \left(\frac{z - z_{\text{ice}}}{k} \right) \right], \quad (\text{S2})$$

we determine the position of the ice interface z_{ice} . Similarly, we make a histogram for the silica atoms and fitting $g(z)$:

$$g(z) = \frac{A}{2} \left[1 + \tanh \left(\frac{z - z_{\text{silica}}}{k} \right) \right], \quad (\text{S3})$$

determining the position of the water-silica interface at z_{silica} . The premelting film thickness is then determined by $h = z_{\text{silica}} - z_{\text{ice}}$.

The friction stress is given by:

$$\sigma_f = - \langle P_{xz} \rangle_t, \quad (\text{S4})$$

The time average from the xz component of the pressure tensor from the MD simulation. Because we freeze and rigidify the bottom and top parts of the system, we must account for the locked-stress contributions from these parts. We use the initial equilibration of 5 ns, during which there is no sliding motion and the friction stress should be zero, to estimate the locked stress. We then correct the friction stress time series and averages used in the main text by subtracting the locked stress from the measured stress. This correction works best for larger stresses that typically occur at higher sliding velocities, and is why we focus on sliding velocities above 0.01 m/s in the main text. Finally, the viscosity of the premelting film is estimated using the relation:

$$\eta = \frac{\sigma_f v}{h}. \quad (\text{S5})$$

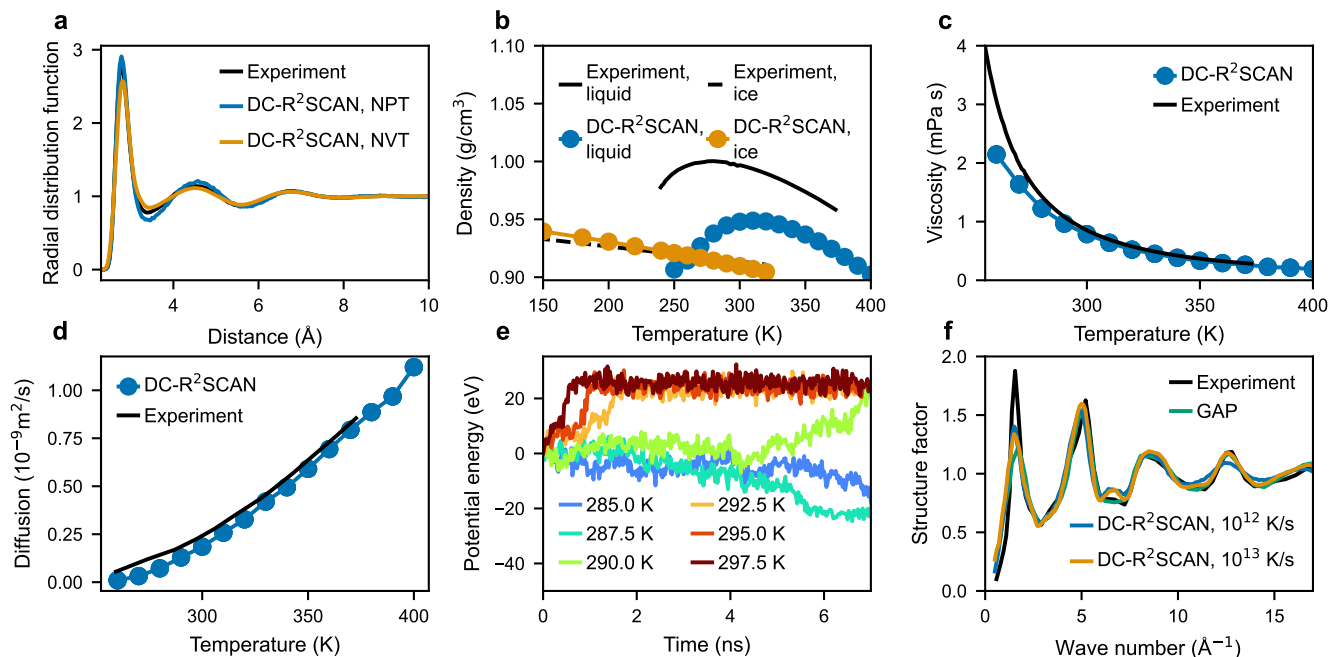


Figure S2 | Validation of DC-R²SCAN MLIP for physical properties. **a** Radial distribution function at 300 K and 0.1 MPa for experiment, and simulations using *NVT* ensemble at experimental density, *NPT* ensemble at 0.1 MPa, 300 K. **b** Density of liquid water and ice from experiments and simulations. **c** Potential energy for liquid-ice coexistence simulations at different temperatures. **d** Diffusion coefficient of liquid water for 0.1 MPa for model and experiments [39–41]. **e** Viscosity of liquid water at 0.1 MPa for model and experiments [42, 43]. **f** Structure factor of amorphous silica from experiments and GAP model [36], and simulations at different annealing rates.

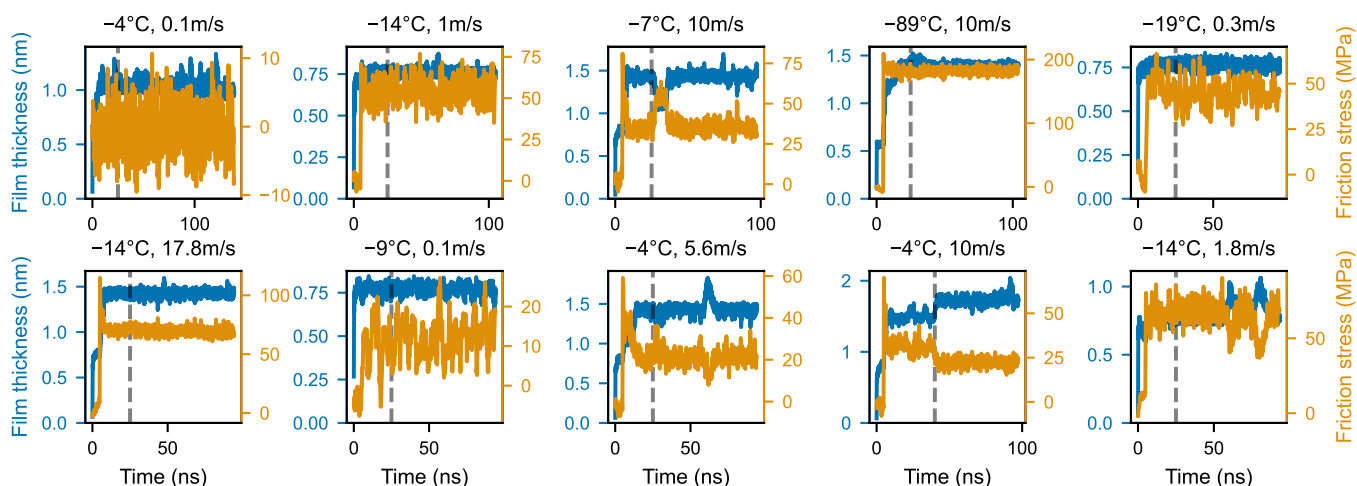


Figure S3 | Nanoscale ice friction time series 1. Each time series is titled with contact temperature in °C with respect to melting point at 289 K and sliding velocity in m/s. Dashed lines indicate the starting frame from which the averages of the steady state are estimated.

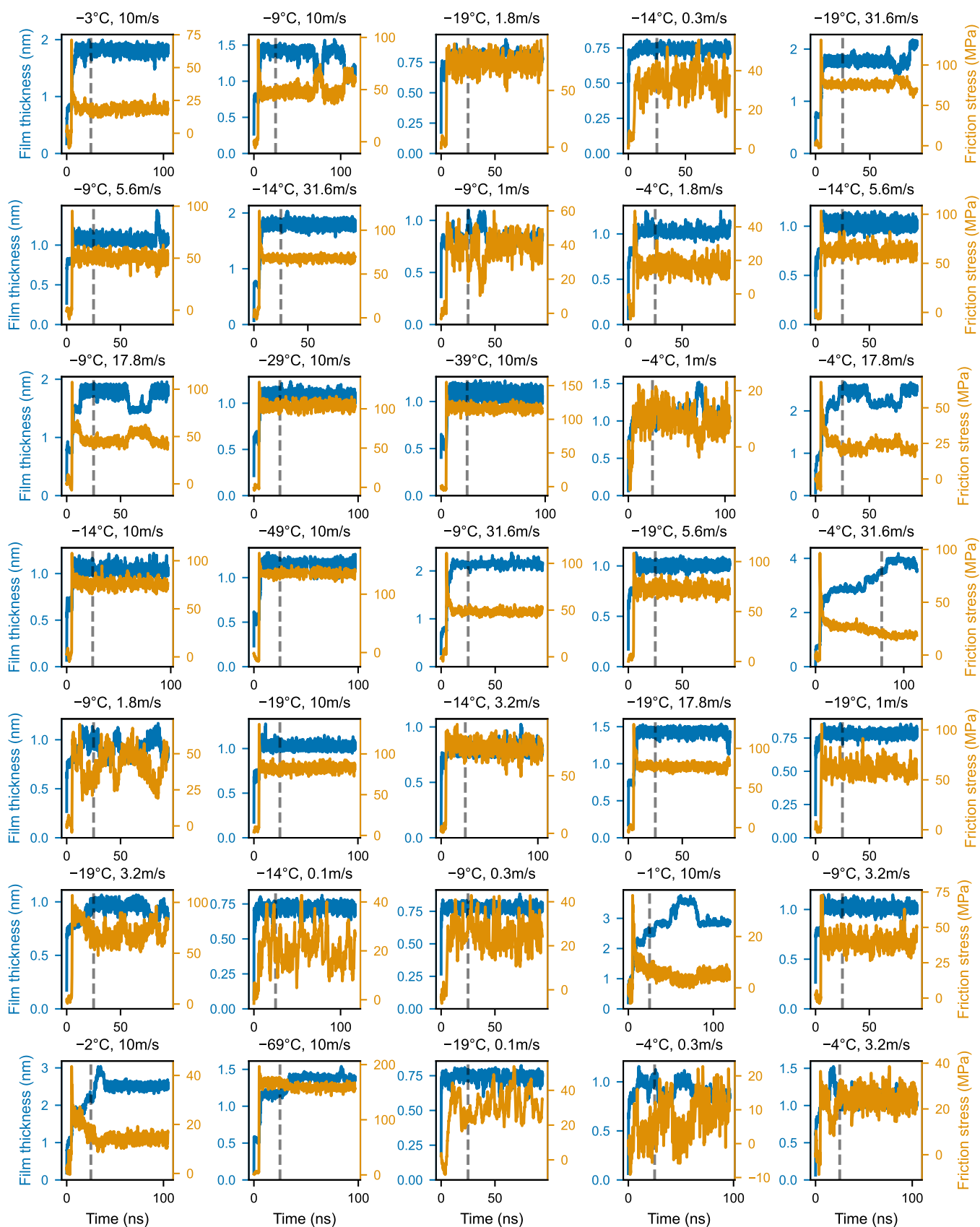


Figure S4 | Nanoscale ice friction time series 2. Each time series is titled with contact temperature in °C with respect to melting point at 289 K and sliding velocity in m/s. Dashed lines indicate the starting frame from which the averages of the steady state are estimated.